Double-electron above threshold ionization of helium

2001 J. Phys. B: At. Mol. Opt. Phys. 34 L69

(http://iopscience.iop.org/0953-4075/34/3/103)

INSTITUTE OF PHYSICS PUBLISHING JOURNAL OF PHYSICS B: ATOMIC, MOLECULAR AND OPTICAL PHYSICS

J. Phys. B: At. Mol. Opt. Phys. **34** (2001) L69–L78 www.iop.org/Journals/jb PII: S0953-4075(01)19632-X

LETTER TO THE EDITOR

Double-electron above threshold ionization of helium

J S Parker, L R Moore, K J Meharg, D Dundas and K T Taylor

Department of Applied Mathematics and Theoretical Physics, The Queen's University of Belfast, Belfast BT7 1NN, UK

Received 30 November 2000

Abstract

We present calculations of intense-field multiphoton ionization processes in helium at XUV wavelengths. The calculations are obtained from a full-dimensional integration of the two-electron time-dependent Schrödinger equation. A momentum–space analysis of the ionizing two-electron wavepacket reveals the existence of double-electron above threshold ionization (DATI). In momentum–space two distinct forms of DATI are resolved, namely non-sequential and sequential. In non-sequential DATI correlated electrons resonantly absorb and share energy in integer units of $\hbar\omega_{\text{laser}}$.

Laser-driven single-photon transitions from the helium ground state to helium doubly excited states are good examples of processes in which coherent, electromagnetic fields are transformed into correlated two-electron atomic states. The distinguishing characteristic of these transitions is the simultaneous absorption of energy by both electrons, accompanied by the absorption of a single unit of angular momentum, $\hbar$, a process that cannot occur unless the two electrons exchange energy during the interaction. Any resonant transfer of population from the ground state to the doubly excited state is mediated simultaneously through the $-(e/mc)\ \boldsymbol{p}.A$ atom–laser interaction and the $e^2/|\boldsymbol{r}_1 - \boldsymbol{r}_2|$ electron–electron interaction in a coherent fashion.

Over the past few decades, synchrotron radiation, owing to its high (XUV) frequency and tunability, has been successfully exploited in the experimental study of this process. A major limitation of synchrotron radiation, aside from its imperfect coherence, has been its extremely low intensity. As a result, multiphoton processes have been inaccessible to experimental study. This is set to change in the near future with the planned completion of the DESY phase 2 free-electron laser (FEL) in the year 2003. The FEL output will be tunable in the range 6.4–20 nm, which is ideal for helium, and will be capable of peak intensities of 5×10^{17} W cm^{-2}.

The theoretical description of these processes has proved as challenging as the experimental problem, although much progress has been reported in the weak field limit appropriate to synchrotron radiation [1–3]. The fact that both atom–laser interactions ($\boldsymbol{p}.A$) and electron–electron interactions ($e^2/|\boldsymbol{r}_1 - \boldsymbol{r}_2|$) come into play simultaneously means that the problem is intrinsically a time-dependent three-body problem. The multiphoton processes which are so well understood in one-electron atoms cannot describe the kind of transitions we are concerned with here.

The problem is still more complex in the high intensity limit, where multiphoton transitions dominate and perturbative methods based on single-photon matrix elements no longer accurately characterize the process. In the intense field limit where non-perturbative effects

are prominent we would expect few approximations to be justified and an accurate description of the atom–laser dynamics would be obtained most reliably from a full-dimensional solution of the three-body Schrödinger equation.

In this letter we present calculations of helium-laser dynamics at high intensity (0.5×10^{16} W cm^{-2} to 4×10^{16} W cm^{-2}) and XUV wavelengths (14–29 nm). The results are obtained by performing a numerical integration of the two-electron time-dependent Schrödinger equation [4, 5]. The main approximation is the assumption of infinite nuclear mass, which along with symmetry due to linear polarization reduces the problem to that of 5 spatial dimensions plus time.

At these high intensities and high frequencies we observe the dramatic production of highly correlated two-electron wavepackets. These two-electron wavepackets in turn are the starting point for additional energy absorption, a process in which the two electrons absorb and share excess energy in units of $\hbar\omega$. We call this process Double-electron Above Threshold Ionization (DATI). Using high resolution calculations of the momentum spectra of the final state, we show that DATI can be resolved into two distinct forms: non-sequential and sequential.

An essential feature of the numerical results is that they are quantitatively accurate with well-established upper bounds on error that are obtained through extensive convergence testing and comparison with known physical results [4–7]. In this letter we limit discussion of the numerics to a few direct tests of the quality of the finite-difference representation of the electrons' mutual Coulomb repulsion, which plays a central role in the double-ionization process described above.

A sensitive indicator of the quality of the numerical representation of correlated two-electron states is provided by measurements of the decay rates and energies of doubly excited states of helium on the finite-difference grid. All helium doubly excited states are auto-ionizing, and the decay rates of these states in the absence of external fields provides a stringent test of the finite-difference representation of the $e^2/|\boldsymbol{r}_1 - \boldsymbol{r}_2|$ electron–electron interaction. The doubly excited state particularly relevant to the present discussion is the 2s2p ^{1}P^o state. We pump population into this state with a short intense pulse tuned to the frequency separation of the initial 1s^2 ^{1}S^e state and the 2s2p state, 20.6 nm (or in atomic units, 2.21 Hartrees). The energy of the 2s2p state is obtained, after the field has been ramped off by a Lanczos-Arnoldi eigendecomposition of the wavefunction [4]. The lifetime of the state is measured by observing the rate of population exiting a sphere of radius 8 au about the nucleus, as the 2s2p decays to a singly ionizing 1skp state of positive momentum k. On a finite-difference grid with a grid point separation of $\delta r = 0.33$ au, the energy and lifetime are measured to be -0.694 au and 720 au respectively, which compare well with the theoretical values of -0.693 au and 732 au [8]. Uncertainties in these measurements are larger than the discrepancies between the measured values and the theoretical values. In the following discussions, all calculations of intense-field double-ionization are performed with grid point separations of $\delta r = 0.25$ au.

The history of the process mentioned in the previous paragraph, from excitation to subsequent decay after the field has returned to zero, can be seen in figure 1. This shows population within 8 au of the nucleus over 140 field periods. The spectrum of the pulse is broad enough, due to its rapid turn-on, to resonantly excite a small amount of population in another nearby auto-ionizing state (the (2s3p + 3s2p) ^{1}P^o) as well. After the field has ramped to zero we see the slow gradual decay of the 2s2p and other states. The inset shows a magnified view of the decay, which displays low amplitude oscillations. The sinusoidal oscillations occur when a coherent superposition of two states decays to a single final state. In the present case, the relevant matrix element has, as its initial state, the coherent superposition of auto-ionizing states and as the final state the wavepacket representing single-electron ionization. The auto-ionizing states that contribute to the decay are the two short-lived states, the 2s2p and the

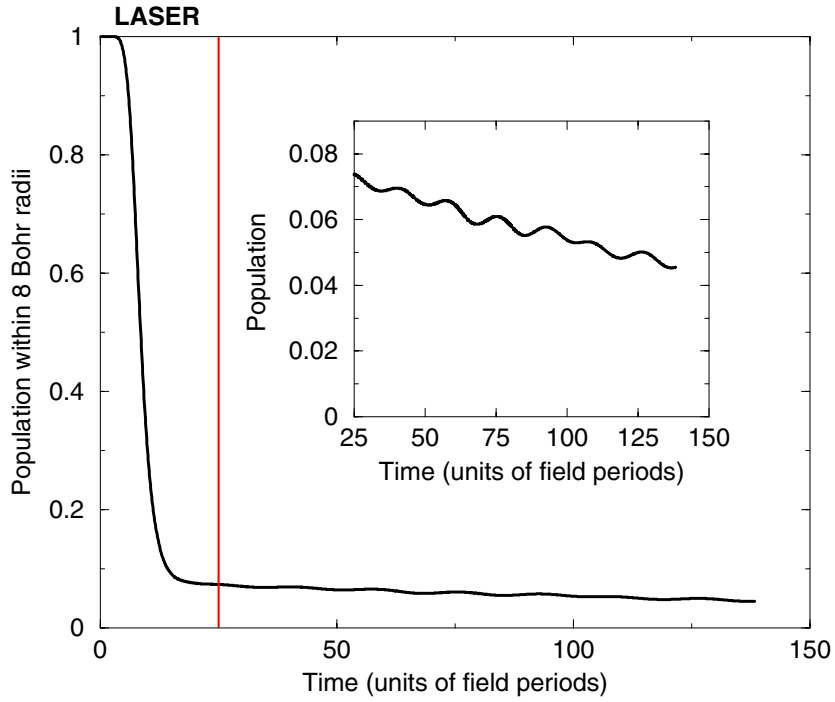

Figure 1. Population within 8 Bohr radii of the nucleus, during excitation with a laser pulse of wavelength 20.6 nm and of peak intensity 4.0×10^{16} W cm^{-2}. The laser pulse is ramped on over 8 field periods and ramped off similarly. The total duration of the laser pulse is 25 field periods, after which there is no laser acting on the system. This point in time is marked by a vertical line. The subsequent decay profile of the population within 8 Bohr radii of the nucleus is magnified in the inset.

(2s3p + 3s2p). The rate of decay is governed by the square modulus of the matrix element, which has cross terms oscillating at the frequency separation of the 2s2p and the (2s3p + 3s2p). This interpretation is confirmed by a measurement of the beat frequency of the decay curve, which exactly equals the frequency separation of the two states.

In this letter we are concerned with intense field double-ionization rather than auto-ionization. Table 1 shows ratios of double-ionization yields to single-ionization yields at the end of 20 field period pulses, for six different frequencies at 0.5×10^{16} and 2×10^{16} W cm^{-2}. Double-ionization yields are obtained by calculating population in doubly ionizing wavepackets as the two electrons are ejected from the atom [5]. It is apparent from table 1 that there is a striking enhancement of the double- to single-ionization ratio at 1.90 and 2.21 au, amounting to an order of magnitude enhancement over the ratios at the lowest and highest frequencies in the table. An independent calculation of He^+ ionization rates, performed using a one-electron model of the $He^+ \rightarrow He^{2+} + e$ process, confirms that these large double- to single-ratios are due to the onset of rapid sequential double-ionization. The $He^+ \rightarrow He^{2+} + e$ ionization rates become so large (for laser frequencies in the neighbourhood of energies that correspond to the 2.0 au ionization potential of He^+), that any He^+ produced through single-ionization is rapidly converted to $He^{2+} + e$. This is in agreement with weak-field ionization cross section calculations at these frequencies [3].

Table 1. Value of ratio He^{2+}/He^{+} for intensities 0.5×10^{16} and 2.0×10^{16} W cm^{-2}.

Frequency (au)	He^{2+}/He^{+}
$I = 0.5 \times 10^{16}$ W cm^{-2}	
1.60	0.06
1.90	0.54
2.21	0.30
2.50	0.15
2.80	0.10
3.20	0.03
$I = 2.0 \times 10^{16}$ W cm^{-2}	
1.60	0.40
1.90	3.74
2.21	3.63
2.50	0.80
2.80	0.42
3.20	0.17

Table 1 illustrates one of the attractive features of atom–laser physics at XUV frequencies, namely the prominence of double-ionization, but the results do not reveal the relative yields of non-sequential and sequential double-ionization. In the following discussion we focus on a single frequency, $\omega = 3.2$ au. At this frequency non-sequential double-ionization can be distinguished unambiguously from sequential and proves to be of comparable prominence.

In order to distinguish non-sequential from sequential, we turn to a momentum–space analysis of the final state. We calculate the momentum–space wavefunction of the ejected electrons at the end of the pulse by Fourier transforming the outgoing wavepackets representing these electrons. To do this a windowing function, similar to the Hamming window commonly used in the Fourier analysis of time-series, is multiplied by the total wavefunction to isolate as far as possible the departing wavepacket from the populated bound states that lie within an 8 Bohr radius of the nucleus. The windowing function is zero within 8 Bohr of the nucleus, and beyond 8 Bohr has a gaussian profile that ramps gradually to unity at 28 Bohr. In order to verify that the results are independent of the window parameters all calculations are repeated with a window that is zero to 20 Bohr from the nucleus and ramps to unity at 40 Bohr. No sensitivity to window position has been observed in the results. The window is applied to both electrons, and has the effect of restricting the analysis to the outgoing waves of doubly ionizing electrons.

The momentum–space wavefunction obtained in this way, $\Phi(\boldsymbol{k}_1, \boldsymbol{k}_2)$, is a 6-dimensional function. The momentum–space wavefunction $\Phi(\boldsymbol{k}_1, \boldsymbol{k}_2)$ is written on a basis set of coupled spherical harmonics $Y_{L,l_1,l_2}(\theta_1, \phi_1, \theta_2, \phi_2)$. This decomposition yields additional information about the absorption of angular momentum by the various ionization processes. In some cases, it is useful to integrate away the angular variables to obtain a 2-dimensional probability distribution

$$P(k_1, k_2) = \alpha k_1^2 k_2^2 \iint \mathrm{d}\Omega_1 \mathrm{d}\Omega_2 |\Phi(\boldsymbol{k}_1, \boldsymbol{k}_2)|^2 \tag{1}$$

where k_1 and k_2 are the radial momentum variables and α normalizes P. The joint probability distribution $P(k_1, k_2)$ conveys information about correlation and kinetic energy. The pulse is ramped off in such a way that the vector potential $A(t)$ and its first two time derivatives go to zero simultaneously, so that at the end of the pulse the canonical momentum $\hbar\boldsymbol{k}$ equals the true momentum and the total kinetic energy of the electrons is $(\hbar^2 k_1^2 + \hbar^2 k_2^2)/2m$.

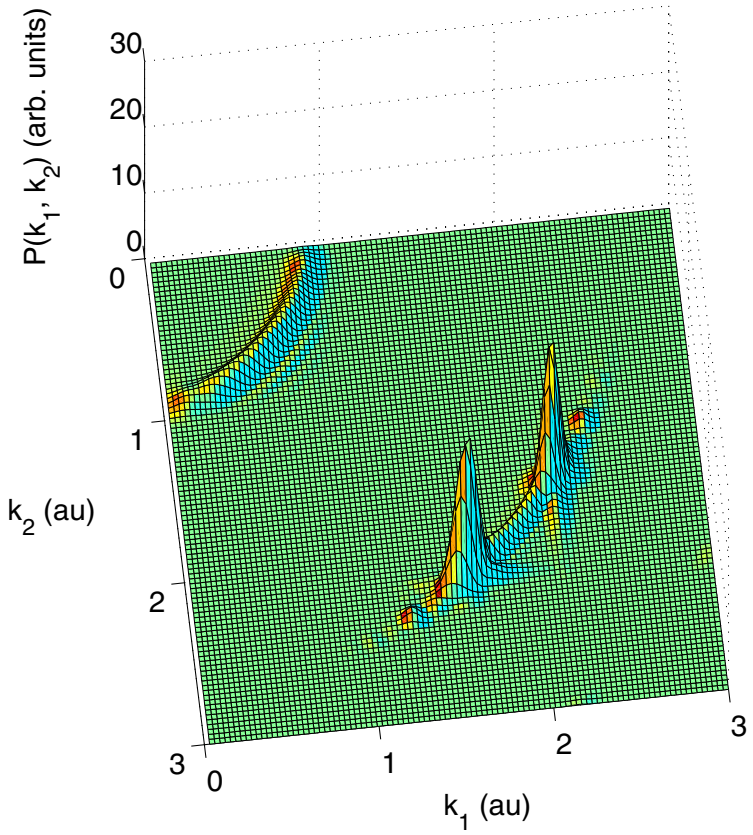

Figure 2. Probability distribution $P(k_1, k_2)$ of doubly ionizing electrons in momentum space after excitation with a 46 field period laser pulse of frequency 3.2 Hartrees and of peak intensity 2.0×10^{16} W cm^{-2}.

Returning briefly to the $\omega = 2.21$ au frequency case involved in figure 1, an important test of the finite-difference momentum–space transformation is provided by the decay dynamics of the 2s2p ^{1}P^o auto-ionizing state. For the purposes of this test the window is chosen to sample regions of single-ionization rather than double-ionization, in other words, regions of space where r_1 is large and r_2 small or vice-versa. The 2s2p ^{1}P^o state (energy -0.693 au) decays to the 1s state (energy -2.0 au) and ejects an electron of energy 1.307 au. As the outgoing waves of this ejected electron depart the Coulomb potential, we expect that the total energy 1.307 au should equal the kinetic energy $k^2/2$ (in au). The measured kinetic energy is 1.337 au. This level of agreement is also typical of the momentum–space calculations of doubly ionizing wavepackets.

We now have the mathematical equipment established and verified so that double-ionization can be satisfactorily discussed. As already stated the discussion will be limited to the case of the laser frequency $\omega = 3.2$ au (14.2 nm), a frequency for which *single-photon* double-ionization from the ground state of He (-2.9037 au) is possible. Figure 2 displays the momentum distribution $P(k_1, k_2)$ at the end of a 46 field period pulse at 2×10^{16} W cm^{-2}. The grid point separation is $\delta r = 0.25$ Bohr, and the volume of integration is a sphere of radius 125 Bohr.

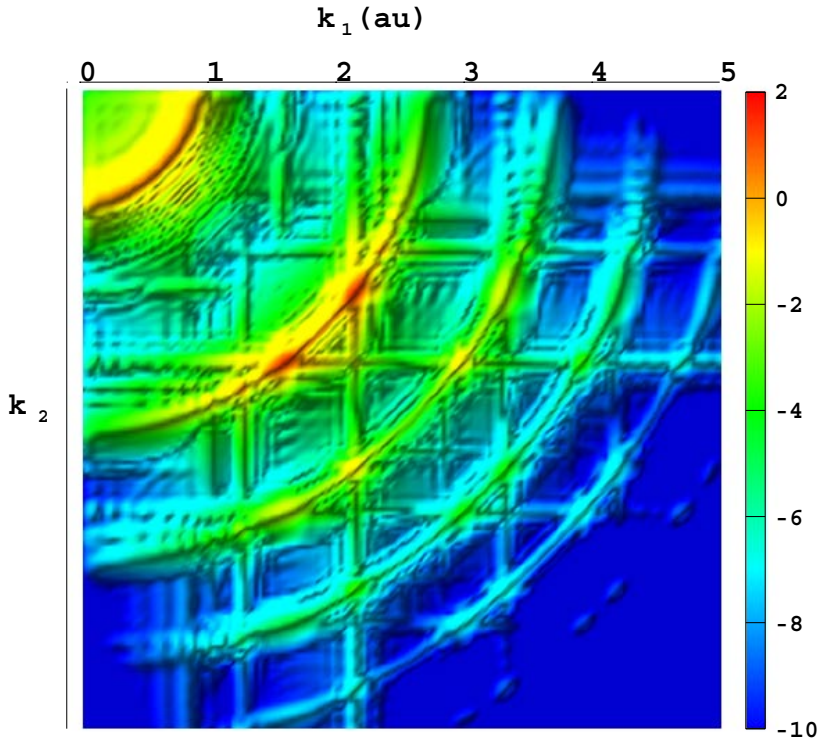

Figure 3. Log plot of the probability distribution $P(k_1, k_2)$ of doubly ionizing electrons in momentum space after excitation with a 46 field period laser pulse of frequency 3.2 Hartrees and of peak intensity 2.0×10^{16} W cm^{-2}. The units are arbitrary and the colour scale is mapped over 12 decades in magnitude.

The most prominent features of figure 2 are a ring at low momenta and lobes at higher momenta. The circular ring represents doubly ionizing electrons of approximately constant total kinetic energy: $k_1^2 + k_2^2 =$ constant. An estimate of the kinetic energy of the two ejected electrons represented by this ring is obtained from

$$\iint \hbar^2 \frac{k_1^2 + k_2^2}{2m} P(k_1, k_2) \mathrm{d}k_1 k_2 \tag{2}$$

which confirms that it is nearly $\hbar\omega$ in energy above the initial $1s^2\ {}^1S^e$ state and hence corresponds to the first ionization peak. In the case of the lobes at higher momenta, the two electrons partition a larger energy in unequal but well-defined amounts. We examine these structures in more detail by taking the logarithm. The result is shown in figure 3.

On a logarithmic scale, figure 3, it is now clear that the twin-lobed ionization peak is part of a larger structure composed of a circular arc and straight lines. Figure 3 is a density plot of the momentum spectrum $P(k_1, k_2)$, calculated as described above. The circular arc satisfying $k_1^2 + k_2^2 =$ constant is the signature of a resonant double-ionization process in which the two electrons are strongly correlated. In other words, if one electron is ejected with momentum k_1, then the other is constrained to $k_2 = \sqrt{(\text{constant} - k_1^2)}$ and the joint probability distribution

$P(k_1, k_2)$ cannot be decomposed into sums of products of functions like $P_1(k_1)$ and $P_2(k_2)$. It is also clear that linear shaped structures pass through the twin-lobed ionization peak. The linear shaped structures parallel to the k_1 or k_2 axis satisfying $k_1 = C_1$ or $k_2 = C_2$ (where $C_{1,2}$ are constants) are the signatures of an uncorrelated process, in which one electron, say electron 1, absorbs a constant momentum C_1 while the second electron absorbs a broad spectrum of momentum as though it is responding to the field independently of electron 1.

As remarked above, the kinetic energy of the first circular arc, $(\hbar^2 k_1^2 + \hbar^2 k_2^2)/2m$, is a constant $\hbar\omega$ above the helium ground state, where ω is the laser frequency 3.2 au. At higher momenta additional rings of constant energy appear. It will be shown below that the energy separation of these arcs is $\hbar\omega$. We call this process non-sequential double-electron above threshold ionization (NS-DATI).

We begin by discussing the linear structures in figure 3. It is straightforward to show that these are due to the above threshold ionization of He^+. In other words they are due to a sequential process in which the two electrons absorb energy independently of each other. The first electron is ejected from neutral He to produce ground state He^+, followed by the absorption of energy in integer multiples of $\hbar\omega$ by the ground state of He^+. Consider the most prominent vertical line in figure 3, the line of constant k_1 with k_1 equal to about 2.15 au. The kinetic energy of this plane wave ($k_1^2/2$ in au) is about 2.31 au. We would expect that a singly-ionizing electron from neutral He would have a total energy of $3.2 - 0.9037 = 2.2963$ au. Asymptotically, far from the atomic potential, this electron's kinetic energy should equal its total energy. Along the line of constant k_1 we see lobes representing resonant ionization. These occur at integer multiples of $\hbar\omega$ above the -2.0 au ground state energy of He^+. Parallel to this line, at $k_1 = 3.3$ au there is another vertical line. Here $k_1^2/2 = 5.45$ au corresponds to the absorption of $2\hbar\omega : 2(3.2) - 0.9037 = 5.4963$ au. In this latter case, (k_1 constant at 3.3 au), both electrons can absorb $2\hbar\omega$ or more. We call this sequential process S-DATI. The same behaviour is observed with the two electrons exchanged.

This finding can be verified quantitatively by comparing the two-electron calculation described above, (along a line of constant k_1), with a purely one-electron calculation of ATI in He^+ ($He^+ \rightarrow He^{2+} + e$) that uses the same integration parameters. Comparison of the kinetic energy distributions of the ejected electrons confirms that the two-electron and one-electron (He^+) atoms exhibit similar patterns of energy absorption with ionization peaks in identical positions. Kinetic energy distributions are calculated directly from the momentum distributions. The quantity plotted in figure 4 as a function of kinetic energy K is the total population such that $(k_1^2 + k_2^2)/2$ is in the range $[K - \delta K, K + \delta K]$ where $\delta K = 0.1$ au. In the case of the two-electron integration only k_2 varies and k_1 is constant. In other words, only population along the vertical line satisfying $k_1^2/2 = 2.31$ au of figure 3 is used. Figure 4 shows (as a dashed line) the kinetic energy distribution of the ejected electron in the one-electron integration ($He^+ \rightarrow He^{2+} + e$) compared with that (as a full line) of the two-electron calculation along a line of constant k_1 ($k_1^2/2 = 2.31$ au). The only major difference between the two calculations is the initial state. In the one-electron case, the initial state is the fully populated 1s ground state of He^+, whereas in the two-electron case the He^+ 1s state is only gradually populated during the pulse, hence different ionization yields are possible in the two cases.

In figure 4 it is apparent that both the two- and one-electron cases, the ionization peaks occur near the vertical lines, which are placed at integer multiples of $\hbar\omega$ above the -2.0 au ground state energy of He^+. Between the peaks, the off-resonant ionization is several orders of magnitude lower than the peaks, but still substantial enough to give rise to the linear structures in figure 3.

The kinetic energy distributions of figure 4 are a useful means of analysing the outgoing wavepackets of the ejected electrons, but the relationship between the ejected electron's total

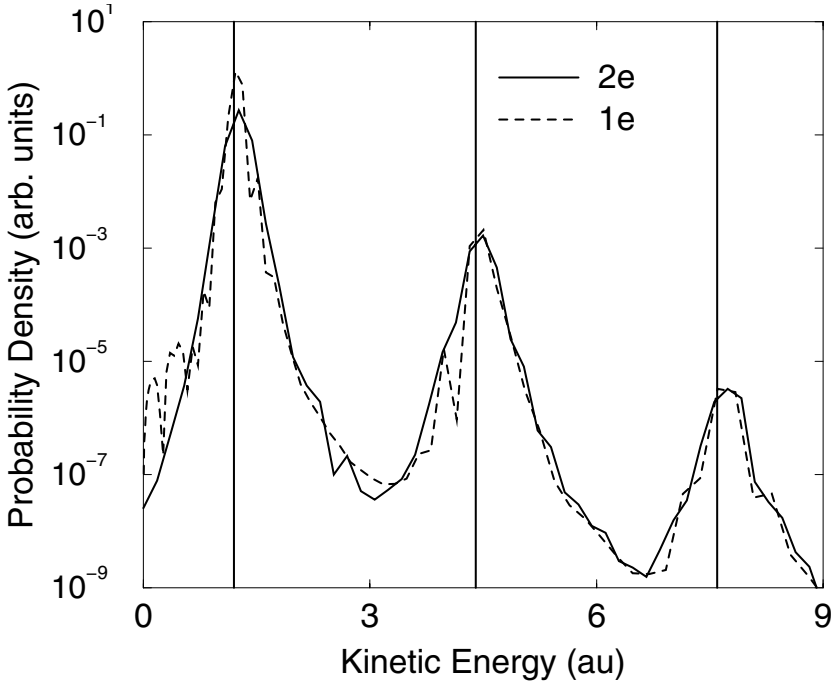

Figure 4. Kinetic energy distribution of ionizing wavepackets for a 46 field period laser pulse of frequency 3.2 Hartrees and of peak intensity 2.0×10^{16} W cm^{-2}. The full curve is the distribution calculated from the full two-electron integration and is obtained by taking a slice through the joint probability distribution $P(k_1, k_2)$ at $k_1 = 2.15$ au. It is the kinetic energy distribution for sequentially ionizing wavepackets in He. The dashed curve is the distribution for ionizing wavepackets in the He^+ calculated by a purely one-electron integration for $He^+(He^+ \rightarrow He^{2+} + e)$.

energy and its kinetic energy is not immediately clear. Because ponderomotive shifts and AC Stark shifts are negligible on the scale of figure 4, we would expect that the total energy would peak exactly where the vertical lines are drawn, at integer multiples of $\hbar\omega$ above the ground state energy. In figure 4 the first two peaks exhibit a perceptible positive shift of about 0.1 au, or 3% of $\hbar\omega$, and the third a somewhat larger shift. We can verify that most of this error is due to the coarseness of the finite-difference grid ($\delta r = 0.25$ au) by reducing δr to 0.15 au and then to 0.05 au in the one-electron integration. As δr is decreased, all three peaks move near to their expected positions, with the largest discrepancies smaller than 0.03 au. The larger the energy of the peak, the greater the finite-differencing error, due to the small de Broglie wavelengths of high energy plane waves. For example, the highest energy peak in figure 4 represents plane waves of wavelength approximately equal to 1.6 Bohr, which comprises about 6 grid points per wavelength. At $\delta r = 0.05$ au we can detect the contribution of the Coulomb potential to the kinetic energy distribution. The ejected electron's kinetic energy is expected to equal the total energy only after it has climbed out of the potential well and travels as a free electron far from the atom. If we make the integration volume substantially larger and use the Fourier transforming window to sample outgoing waves only beyond 30 au from the nucleus, then no shift is observed and the ionization peaks appear exactly $N\hbar\omega$ above the ground state. In practice, we can only perform the calculation to this level of accuracy with the one-electron ($He^+ \rightarrow He^{2+} + e$) integration.

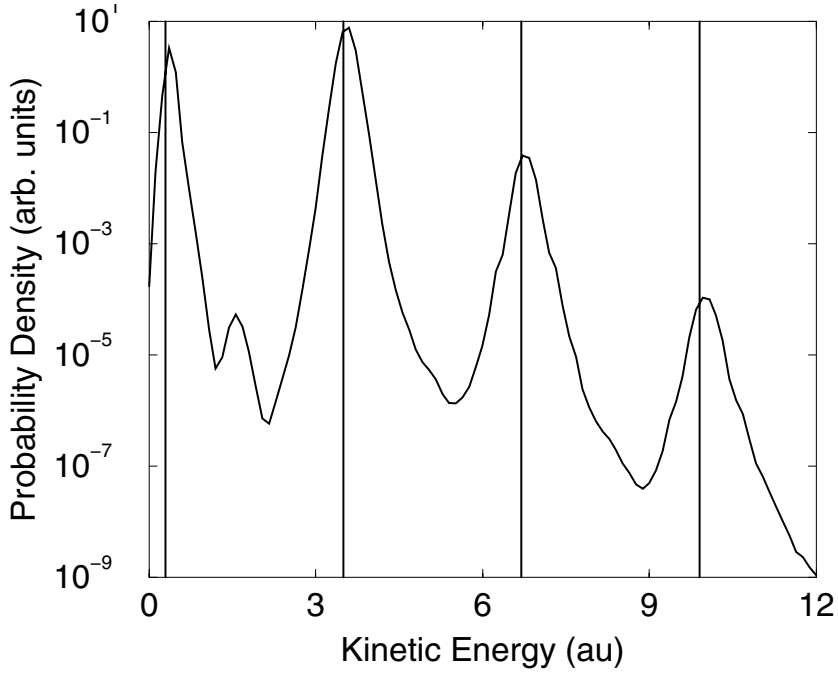

Figure 5. Total kinetic energy distribution of doubly ionizing electrons in He after excitation with a 46 field period laser pulse of frequency 3.2 Hartrees and of peak intensity 2.0×10^{16} W cm^{-2}.

Figure 5 shows the total kinetic energy distribution, calculated using the entire final state momentum distribution shown in figure 3. In this case the kinetic energy is $(k_1^2 + k_2^2)/2$ (rather than $k_2^2/2$ as in figure 4) and the quantity plotted as a function of K is total population found to be within a distance δK of K, where $\delta K = 0.1$ au. We see now that the peaks in kinetic energy occur near the vertical lines which are placed at integer multiples of $\hbar\omega$ above the -2.9037 au ground state of neutral helium. Again there is a slight but perceptible positive shift due to the coarseness of the grid (here $\delta r = 0.25$ Bohr), which decreases as δr decreases.

It is clear from figure 3 that the lowest energy ionization ring, at $\hbar\omega$ above the ground state, nowhere intersects the linear structures representing sequential ionization of He^+, and therefore receives no resonant contributions from sequential processes. A decomposition of the wavefunction in terms of spherical harmonics confirms that this ring lies almost entirely in the $L = 1$ partial wave, where $\hbar L$ is total angular momentum. The first ring therefore represents an almost pure example of non-sequential single-photon double-ionization of helium. The partial wave decomposition similarly confirms that the second ring is substantially contained in the $L = 2$ partial wave, the third in the $L = 3$, and so on. This is in agreement with the usual observed behaviour in one-electron resonant processes in which dipole moments favour absorption of $\hbar$ angular momentum with the absorption of each $\hbar\omega_{\text{laser}}$ of energy.

We have presented calculations of double-electron ionization in helium at frequencies and intensities in the range free-electron lasers are expected to be capable of generating in the near future. We have discussed in particular the high frequency limit ($\hbar\omega > 2.9037$ au) in which the two electrons absorb enough energy to ionize simultaneously, while absorbing only $\hbar$ angular momentum from the field, a process that cannot occur unless there is a transfer of energy between the electrons during the interaction through mutual electrostatic repulsion.

We have chosen to explore the high intensity limit ($I \approx 10^{16}$ W cm^{-2}) appropriate to free-electron lasers, where non-perturbative multiphoton processes are expected to dominate, and a full-dimensional time-dependent treatment of the Schrödinger equation is a requirement for reliable calculations. A momentum–space analysis of the final-state wavefunction reveals that the ionization process described above is the first step in a resonant process we have called non-sequential double-electron above threshold ionization (NS-DATI). In the NS-DATI process the two electrons simultaneously absorb energy in integer units of $\hbar\omega$ and are ejected from the atom in a correlated two-electron wavepacket. The momentum–space picture nicely distinguishes this process from the less interesting sequential double-ionization of He, an uncorrelated process which can be accounted for entirely with one-electron models.

KTT acknowledges helpful discussions with Professor Peter Lambropoulos. This research was supported by grants from the UK Engineering and Physical Sciences Research Council providing support for JSP and DD together with high-performance computer resources at the Computing Service for Academic Research, University of Manchester. LRM and KJM acknowledge receipt of research studentships provided by the Department of Higher and Further Education, Training and Employment.

References

[1] Pont M and Shakeshaft R 1997 Double Photoionization of Helium *Proc. of Photon and Electron Collisions with Atoms and Molecules* (PECAM-II) Ed P G Burke and C J Joachain (New York: Plenum)
[2] Tanner G, Richter K and Rost J M 2000 *Rev. Mod. Phys.* **72** 498
[3] Kornberg M A and Lambropoulos P 1999 *J. Phys. B: At. Mol. Opt. Phys.* **32** L603
Nikolopoulos L A A and Lambropoulos P 2001 Multichannel theory of two-photon single and double ionization of Helium *J. Phys. B: At. Mol. Opt. Phys.* submitted
[4] Smyth E S, Parker J S and Taylor K T 1998 *Comput. Phys. Commun.* **114** 1
[5] Parker J S, Moore L R, Dundas D D and Taylor K T 2000 *J. Phys. B: At. Mol. Opt. Phys.* **33** L691
[6] Parker J S, Glass D H, Moore L R, Smyth E S, Taylor K T and Burke P G 2000 *J. Phys. B: At. Mol. Opt. Phys.* **33** L239
[7] Parker J S, Moore L R, Smyth E S and Taylor K T 2000 *J. Phys. B: At. Mol. Opt. Phys.* **33** 1057
[8] Scrinzi A and Piraux B 1998 *Phys. Rev.* A **58** 1310